



FINITE ELEMENT APPROACH TO ANALYZE STRUCTURAL DISCONTINUITIES ASSOCIATED WITH SHIP HULL

Kazi Naimul Hoque^{*} and Md. Shahidul Islam¹

¹Department of Naval Architecture and Marine Engineering, Bangladesh University of Engineering and Technology (BUET), BUET Central Road, Dhaka-1000, Bangladesh, *kazinaim@name.buet.ac.bd, shahid777@name.buet.ac.bd

Abstract:

The finite element method (FEM) is widely recognized as a powerful numerical analysis technique for approximating solutions in structural mechanics. Addressing the configuration of plate-type structures, particularly those with discontinuities, is crucial not only in ship and aircraft construction but also in various other fields. Structural discontinuities occur when there are sudden changes in the cross-section of structural members due to material imperfections or high-stress areas. This paper focuses on the fundamental principles of FEM for solving two-dimensional plane stress problems and analyzing stresses such as normal stress, shear stress, and von-Mises stress at the four integration points (Gauss points) in different sections of ship structures, particularly in vulnerable regions. To address structural discontinuity problems in various ship structures, a finite element program utilizing object-oriented techniques was developed, employing four-node quadrilateral elements. The analysis results of gauss point stresses obtained from the developed program were validated against a commercial finite element analysis software to ensure accuracy and reliability. Additionally, a mesh viewing program has been developed in the Python programming language to enable the visualization and analysis of the generated mesh using the developed object-oriented finite element program.

Keywords: Plane stress, structural discontinuities, finite element analysis, von-Mises stress, shear stress, object oriented programming.

NOMENCLATURE

Q	global displacement vector	Π	potential energy
F	global load vector	σ_Y	yield stress
q	element displacement vector	σ_x	normal stress along x-direction
ξ, η	natural coordinates	σ_y	normal stress along y-direction
D	stress-strain displacement matrix	τ_{xy}	shear stress
B	element strain displacement matrix	σ_{mises}	von-Mises stress
K	element stiffness matrix	ν	Poisson's ratio
E	modulus of elasticity	σ	stress

1. Introduction

A structural discontinuity arises whenever the cross-sectional profile of a structural member undergoes an abrupt alteration, as seen in instances such as deck openings, hatch and machinery openings, access points on sidewalls, web plate cutouts, and oil holes in crankshafts, and among others. These structural irregularities lead to changes in the stress distribution within a structure, resulting in the introduction of stresses around hole perimeters or at the extremities of cracks. Various professionals, including hydrodynamicists, mathematicians, offshore and ocean engineers, as well as naval architects, have all delved into extensive research to comprehend the implications of structural discontinuities. In general, the assessment of stress in these situations has been performed through either analytical or experimental means, a process that can be resource-intensive and time-consuming, particularly when grappling with complex discontinuity configurations. The complexity of these discontinuity configurations often rendered it exceedingly difficult to devise a suitable solution.

Bea et al. (1995) conducted an extensive investigation into the significance of fatigue cracks and corrosion in tankers. Baumann (1997), using finite element modeling, assessed the structural integrity of a hull girder penetration and a short longitudinal bulkhead. Notably, research addressing the impact of corrosion and fatigue cracking on ship hull structural integrity was limited, as pointed out by Soares and Garbatov (1998). Niu (1998) conducted an in-depth study on stress analysis within the context of an airframe structure. Due to the considerable uncertainties associated with these failure modes, modeling the effects of corrosion and fatigue cracking on ship hull structural integrity presents a formidable challenge.

The applicability of object-oriented programming (OOP) techniques for the efficient and understandable structure of the data in numerical analysis codes was investigated. The excessively sequential, and thus too restricting, aspect of traditional algorithm implementation was addressed by Baugh and Rehak (1990), who also introduced a more flexible data flow organization. The first attempts to design finite element software architecture were presented by Forde et al. (1990), Zimmermann et al. (1992), and Dubois-Pelerin et al. (1992). Fenves (1990), Miller (1991), Desjardins, and Fafard (1992) were responsible for other advancements. With the work of Mackerle (2000), object-oriented notions were applied to finite element programming to a great deal of attention. In-depth analysis of the object-oriented framework for finite element programming has been conducted by Martha (2002). The fundamental concepts of applying object-oriented techniques to the finite element method (FEM) produced a code that was extremely modular, simple to comprehend, and extensible. A study on the two-dimensional plane stress and plane strain analysis of structural discontinuities related to ship structures was conducted by Hoque (2016). On the crack and corrosion propagation of marine structures constructed using marine materials, several research studies were conducted (Presuel-Moreno et al., 2022, 2018; Presuel-Moreno and Hoque, 2023, 2019; Hoque, 2020). Using the FEM, Thohura and Islam (2013) investigated the impact of mesh quality on the stress concentration factor for plates with holes. With the aid of the Python programming language, Edholm (2013) carried out finite element analysis for the visualization of quadrilateral and triangular mesh.

The OOP method was employed in this study. When developing large, complex programs-like the FEM, that should handle various element types, constitutive models, and analysis algorithms-the OOP is especially helpful. In this work, the four integration points (gauss points) were used to analyze stresses such as normal stress, shear stress, and von-Mises stress for various ship structure components. A finite element program for four node quadrilateral elements was developed using an OOP technique to investigate structural discontinuity problems for different ship sections. The commercial finite element analysis (FEA) software SIMULIA ABAQUS was used to validate the study's findings regarding gauss point stresses for different models derived from the developed program.

2. Basic Formulation

2.1 Finite element modeling

FEM is the dominant discretization technique in structural mechanics. The basic concept in FEM is the subdivision of a region into disjoint (non-overlapping) components of simple geometry called finite element or element for short. For two-dimensional modeling the most employed elements are linear or quadratic triangles and quadrilaterals. In two-dimensional problems, each node is permitted to displace in two directions. Thus, each node has two degrees of freedom. So, the displacement components of node j are taken as Q_{2j-1} in the x direction and Q_{2j} in the y direction. And the global displacement vector can be represented as

$$\{Q\} = [Q_1, Q_2, \dots, Q_N]^T \tag{1}$$

and global load vector,

$$\{F\} = [F_1, F_2, \dots, F_N]^T \tag{2}$$

where N is the number of degrees of freedom (d.o.f.), which is defined as the flexibility of the nodes to displace in permitted numbers of direction. Thus, in two-dimensional problem, as the nodes are permitted to displace in both $\pm x$ and $\pm y$ direction, hence each node has two degrees of freedom.

2.2 Shape functions

A general quadrilateral element is considered as shown in Figure 1(a), which has local nodes numbered as 1, 2, 3 and 4 in a counterclockwise fashion and (x_i, y_i) are the coordinates of node i . The vector $\{q\} = [q_1, q_2, \dots, q_8]^T$ represents the element displacement vector. To develop the shape functions, a master element is considered (Figure 1(b)) having a square shape and being defined in ξ -, η - coordinates (or natural coordinates). The Lagrange

shape functions, where $i = 1, 2, 3$ and 4 , are defined such that N_i is equal to unity at node i and is zero at other nodes. In particular:

$$N_1 = \begin{cases} 1, & \text{at node 1} \\ 0, & \text{at node 2, 3 and 4} \end{cases} \quad (3)$$

The requirement that $N_1 = 0$ at nodes 2, 3 and 4 is equivalent to requiring that $N_1 = 0$ along edges $\xi = +1$ and $\eta = +1$ (Figure 1(b)).

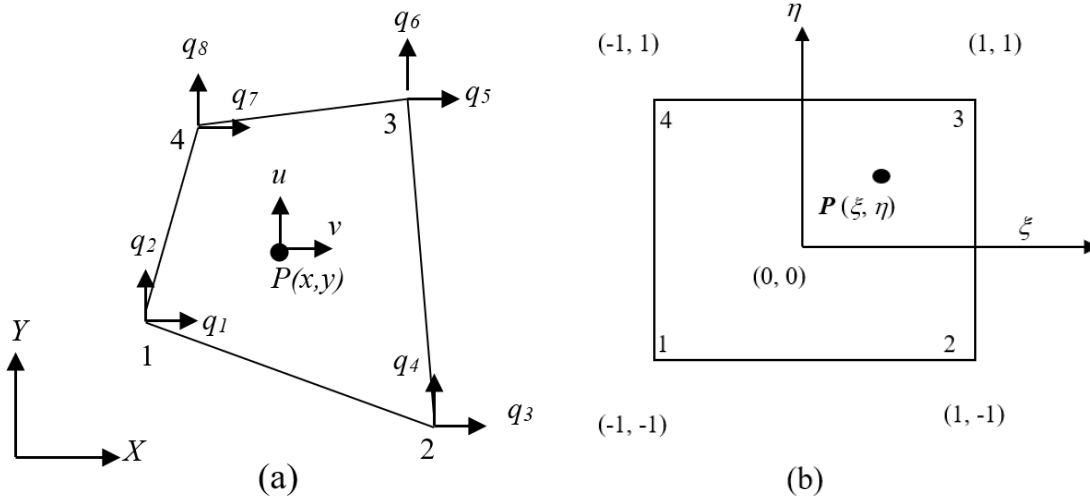


Figure 1: a) Four-node quadrilateral element; b) The quadrilateral element in ξ, η space (master element)

All the four shape functions can be written as

$$\begin{aligned} N_1 &= \frac{1}{4}(1 - \xi)(1 - \eta) & N_2 &= \frac{1}{4}(1 + \xi)(1 - \eta) \\ N_3 &= \frac{1}{4}(1 + \xi)(1 + \eta) & N_4 &= \frac{1}{4}(1 - \xi)(1 + \eta) \end{aligned} \quad (4)$$

2.3 Treatment of boundary conditions

In dealing with the proper boundary condition and deriving the equilibrium equations the penalty approach was used. Consequently, the equations of equilibrium can be obtained by minimizing with respect to Q , the potential energy Π subject to the boundary conditions. Boundary conditions are usually of the type,

$$Q_{p1} = a_1, Q_{p2} = a_2, \dots, Q_{pr} = a_r \quad (5)$$

where, P_1, P_2, \dots, P_r are denoted to be the degrees of freedom and r is judged to be the number of supports in the structure. The requirement that the potential energy Π takes on a minimum value is obtained from the equation.

$$\frac{d\Pi}{dQ_i} = 0 \quad i = 2, 3, \dots, N \quad (6)$$

Applying these boundary conditions and using the Equation (6) the finite element equations can be expressed in the matrix form as,

$$[K]\{Q\} = \{F\} \quad (7)$$

where, $[K]$ and $\{F\}$ are the modified stiffness and load matrices. For matrix solving, conjugate gradient method was used.

2.4 Element stress calculation

Equation (7) can be solved for the displacement vector $\{Q\}$ using Gaussian elimination. As the $[K]$ matrix is a nonsingular one, the boundary condition can be considered of specified properly. Once $\{Q\}$ has been determined, the element stress can be evaluated using the equation derived from Hooke's law,

$$\{\sigma\} = [E][B]\{q\} \quad (8)$$

where $[B]$ is the element strain-displacement matrix and $\{q\}$ is the element displacement vector for each element, which is extracted from $\{Q\}$, using element connectivity information.

2.5 Von-Mises stress

The von-Mises stress is a combined representation of all the stresses, including normal stress in three directions and all three shear stresses, acting at a specific location. When the von-mises stress surpasses the yield strength, the material yields at that location. Similarly, if the von-Mises stress exceeds the ultimate strength, the material ruptures at that location. The failure criterion dictates that the von-Mises stress (σ_{mises}) should be lower than the yield stress (σ_Y) of the material. This criterion can be expressed in the form of an inequality as follows:

$$\sigma_{\text{mises}} \leq \sigma_Y$$

The von-Mises stress σ_{mises} is given by,

$$\sigma_{\text{mises}} = \sqrt{(\sigma_x + \sigma_y)^2 - 3(\sigma_x \sigma_y - \tau_{xy}^2)} \quad (9)$$

3. Research Methodology

Over the past few years, the utilization of object-oriented concepts in finite element programming has gained significant attention. One of the key advantages of adopting an object-oriented approach is the simplicity and naturalness of program expansion, as new implementations have minimal impact on the existing code. This maximizes code reusability. Additionally, compared to classical structured programming, the use of OOP allows for a closer integration between theory and computer implementation. OOP proves particularly beneficial in the development of large and complex programs, such as finite element systems that need to handle different element types, constitutive models, and analysis algorithms. However, to fully exploit the advantages of the object-oriented approach, a comprehensive understanding of the employed methodology and substantial efforts in program organization are required. The objective of this work is to present an ongoing endeavor in developing a finite element analysis system based on object-oriented programming, referred to as FEMOOP, which encompasses the overall architecture of the system.

4. Object-Oriented Finite Element Programming

Before exploring the class organization of the FEMOOP program, it is crucial to recognize that nonlinear finite element analysis entails computations at three distinct levels: the structure level, the element level, and the integration point level. At the structure (or global) level, various algorithms are employed to analyze the problem, such as linear static, linearized buckling, linear dynamic, nonlinear path-following, and nonlinear dynamic analyses. These algorithms are implemented using global vectors and matrices and are independent of the specific types of elements and materials used in the analysis. The element level primarily focuses on computing element vectors and matrices, such as the internal force vector and stiffness matrix. These computations are necessary for assembling the global vectors and matrices used by the analysis algorithms. Importantly, the computation of these element vectors and matrices remains completely independent of the chosen analysis algorithm.

The interconnection between the global and element levels operates in two directions. In the upward direction, global vectors and matrices are computed by aggregating the contributions from individual elements. In the downward direction, element displacements are extracted from the global displacement vector. These communications tasks rely on nodal degrees of freedom and element connectivity. Lastly, at the integration point level, the computation of stress vectors and tangent constitutive matrices takes place. These quantities are utilized in the calculation of element vectors and matrices. However, they do not rely on the specific element formulation if the essential input data for stress computation, such as strain components, are provided.

Previous studies have extensively examined the convergence characteristics of two-dimensional solutions for elastic continuum problems using both quadrilateral and triangular elements. These studies have identified several significant factors that influence the convergence properties of finite element solutions. These factors include the basic shape of the elements, element distortion, polynomial order of the elements, completeness of polynomial functions, integration techniques, and material incompressibility.

In general, it is widely accepted that quadrilateral elements outperform simplex triangular elements. Quadrilateral elements are preferred for two-dimensional meshes due to their superior accuracy and efficiency, while hexahedral elements are favored for three-dimensional meshes. This preference is evident in structural analysis and extends to various engineering disciplines.

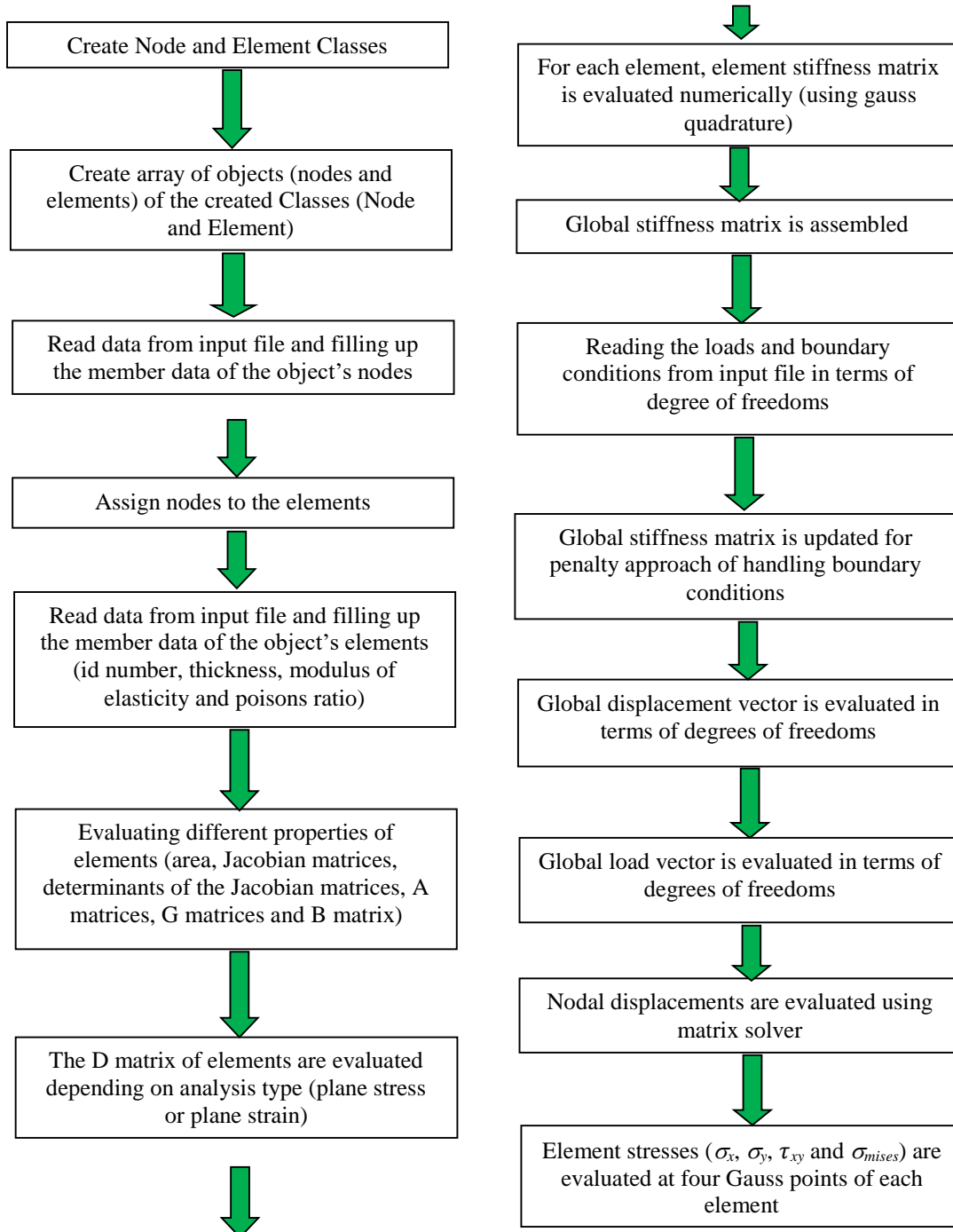


Figure 2: Flow chart of the developed program

However, it is also acknowledged that triangular elements, especially those with higher order displacement assumptions, can provide acceptable accuracy and convergence characteristics. Nonetheless, one notable drawback of triangular elements is the possibility of mesh locking caused by material incompressibility. This issue represents a significant limitation when utilizing triangular elements in certain applications.

The object-oriented code utilized in this research features the creation of two distinct classes: "Node" and "Element." The "Node" class encompasses various attributes such as coordinates, displacements, boundary conditions, and loads, with member functions responsible for reading and computing these attributes. In a similar fashion, the "Element" class comprises several attributes like constituent nodes, element thickness, and material properties, with its member functions dedicated to reading and computing these properties. Following this, an array of objects derived from these classes is generated, facilitating the assembly of the global stiffness matrix and global load vector. Utilizing the penalty approach to address boundary conditions, the code proceeds to assess nodal displacements and elemental stresses. The flow chart of the developed program is shown in Figure 2.

5. Results and discussion

In this study, the SIMULIA ABAQUS 13.3 version, FEA software, was utilized. The software was employed to examine different plane stress problems associated with ship structures, considering suitable boundary conditions and loadings. Visual representations in the form of images were employed to illustrate the results. The primary focus of analysis was on shear stress and von-Mises stress, specifically at the four integration points in the most vulnerable regions of various structural sections of a ship. Consequently, the obtained stress findings from the FEA software were compared to those derived from the developed program, with the corresponding percentage of error presented for each result.

5.1 Problem statement 1 (rectangular plate)

The first model for the two-dimensional plane stress problem is shown in Figure 3(a). In this model, a rectangular plate section was constrained at the left vertical edge in both x and y direction and a concentrated force of 10,000 N was applied at the right vertical edge. The rectangular plate had a length of 60 mm, a width of 30 mm, and a thickness of 10 mm.

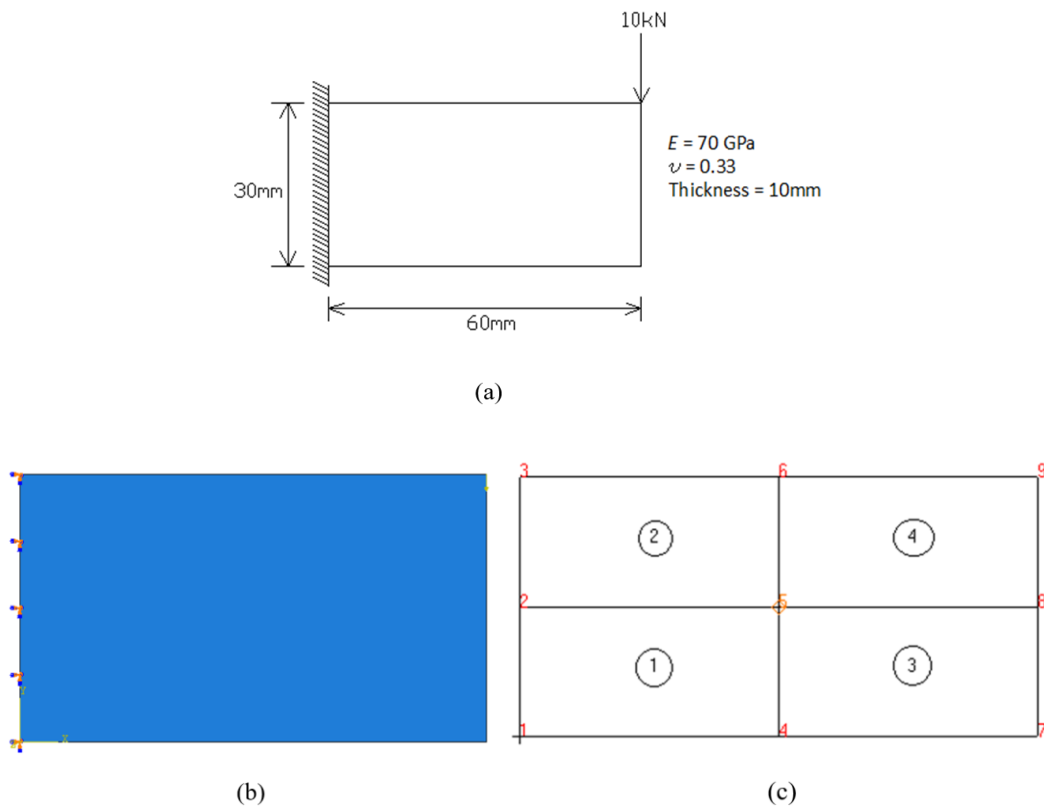


Figure 3: a) Rectangular plate with specifications; b) Application of boundary conditions and loadings; c) Quadrilateral mesh

In the developed program, the data file generated for problem statement 1 using Microsoft Visual Studio C++ software is as follows-

```

TITLE OF PROBLEM
NN NE NM NDIM NEN NDN
ND NL Ps
Node# X Y
Elem# N1 N2 N3 ME NU Thickness
DOF# Displacement 2n-1(x), 2n(y)
DOF# Load 2n-1(x), 2n(y)
9 4 1 2 4 2
6 1 1
1 0 0
2 0 15
3 0 30
4 30 0
5 30 15
6 30 30
7 60 0
8 60 15
9 60 30
1 1 4 5 2 70E3 .33 10
2 2 5 6 3 70E3 .33 10
3 4 7 8 5 70E3 .33 10
4 5 8 9 6 70E3 .33 10
1 0
2 0
3 0
4 0
5 0
6 0
18 -10000
    
```

Here,

- NN = Number of Nodes
- NE = Number of Elements
- NM = Number of Different Materials
- NDIM = Number of Coordinates per Node (e.g., NDIM = 2 for 2-D, or = 3 for 3-D)
- NEN = Number of Nodes per Element (e.g., NEN = 3 for 3-noded triangular element, or = 4 for a 4-noded quadrilateral)
- NDN = Number of Degrees of Freedom per Node (e.g., NDN = 2 for a CST element, or = 6 for 3-D beam element)
- ND = Number of Degrees of Freedom along which Displacement is Specified = No. of Boundary Conditions
- NL = Number of Applied Component Loads (along Degrees of Freedom)
- Ps = No. for Plane Stress/ Plane Strain Analysis (e.g., Ps = 1 for Plane Stress Analysis, or = 2 for Plane Strain Analysis)

ME = Modulus of Elasticity

NU = Poisson's ratio

Using this data file in the developed program, the output file for problem statement 1 is obtained in terms of stresses at the four integration points and displacements at the nodal points.

The execution file is obtained using the Microsoft Visual Studio C++ software.

From the execution file,

Starting time of the program for problem statement 1 = 23:36:06 p.m.

Ending time of the program for problem statement 1 = 23:36:07 p.m.

Time required to execute the output file for problem 1 = (23:36:07 - 23:36:06) p.m.
= 1 second

For the analysis, the model was divided into 4 quadrilateral elements in which there were 9 nodes. The generated quadrilateral mesh for this model is illustrated in Figure 3(c). The modulus of elasticity and Poisson's ratio of the material of the plate were $70 \times 10^3 \text{ N/mm}^2$ and 0.33 respectively. The boundary conditions and loadings were applied using the FEA software as shown in Figure 3(b). Here, the left vertical edge was constrained in both x and y direction, i.e., $U_x = U_y = 0$ and a concentrated downward force was applied at the uppermost point in the right vertical edge.

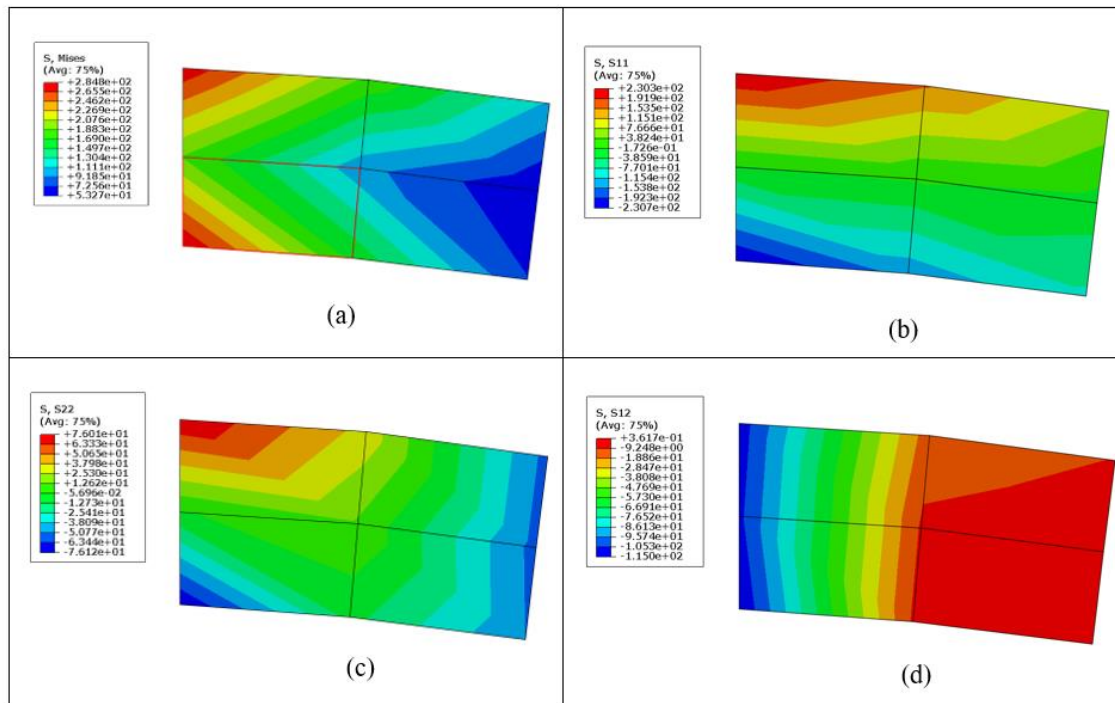


Figure 4: Analysis of rectangular plate section in terms of (a) σ_{mises} , (b) σ_x , (c) σ_y , and (d) τ_{xy}

The FEM analysis (results) of first model in terms of σ_{mises} (von-Mises stress), σ_x (normal stress along x-direction), σ_y (normal stress along y-direction), and τ_{xy} (shear stress), were illustrated in Figure 4(a) to Figure 4(d). From Figure 4, it was found that (a) σ_{mises} was maximum around the region of element no 1 for node no 1 and element no 2 for node no 3, (b) σ_x was maximum around the region of element no 2 for node no 3, (c) σ_y was also maximum around the region of element no 2 for node no 3, and (d) τ_{xy} was maximum around the region of element no 3 for all the quadrilateral nodes and also element no 4 for particularly node no 5, 8 & 9. Comparison of σ_{mises} , and τ_{xy} for different elements and nodes obtained from the developed program and the analysis were shown in Table 1 and Table 2.

When examining σ_{mises} (von-Mises stresses) in Table 1, it became evident that the maximum tensile stress occurred at integration point 1 for element number 1. The developed program yielded a value of 213.369 N/mm^2 , while the analysis provided a value of 213.363 N/mm^2 . These two values were remarkably close, with an error of merely 0.003%. Furthermore, all the stresses were observed to be tensile. It was notable that the results of σ_{mises} exhibited a high level of similarity, with a relatively small percentage of error when comparing the other values in Table 1.

Consistent results regarding σ_{mises} were observed across these investigations (Hoque, 2016; Hoque and Islam, 2023).

Table 1: Comparison of σ_{mises} for rectangular plate section

Element No.	Integration point	σ_{mises} from developed program (N/mm ²)	σ_{mises} from analysis (N/mm ²)	% of error
1	1	213.369	213.363	0.003
	2	160.288	160.280	0.005
	3	53.787	53.779	0.015
	4	141.138	141.135	0.002
2	1	136.963	136.961	0.001
	2	48.536	48.529	0.013
	3	159.952	159.945	0.004
	4	208.324	208.319	0.002
3	1	93.737	93.736	0.001
	2	58.818	58.816	0.004
	3	38.025	38.024	0.005
	4	91.476	91.475	0.001
4	1	92.309	92.307	0.002
	2	69.323	69.321	0.003
	3	94.186	94.183	0.004
	4	120.104	120.101	0.002

Table 2: Comparison of τ_{xy} for rectangular plate section

Element No.	Integration point	τ_{xy} from developed program (N/mm ²)	τ_{xy} from analysis (N/mm ²)	% of error
1	1	-81.288	-81.288	0.000
	2	6.643	6.643	0.007
	3	10.694	10.694	0.004
	4	-77.237	-77.237	0
2	1	-75.577	-75.577	0
	2	14.818	14.819	0.002
	3	12.838	12.838	0.001
	4	-77.558	-77.558	0.001
3	1	-44.190	-44.190	0.001
	2	-13.333	-13.333	0.001
	3	-19.892	-19.892	0.002
	4	-50.749	-50.749	0
4	1	-49.377	-49.376	0.001
	2	-13.392	-13.392	0
	3	-19.875	-19.875	0.001
	4	-55.860	-55.860	0

In case of τ_{xy} (shear stresses), it was observed from Table 2 that the compressive stress was maximum at the integration point 1 for element no 1 which had a value of 81.288 N/mm² obtained from the developed program and 81.288 N/mm² obtained from the analysis. These two values were the same, having an error of 0% which is impressive. The tensile stress was found to be maximum at integration point 2 for element no 2 in which the values were 14.818 N/mm² utilizing the developed program and 14.819 N/mm² obtained from the analysis. These two values of tensile stress were quite close showing an error of 0.002%. In comparison of all other values from Table 2, it was observed that the results of τ_{xy} (shear stress) were almost identical showing relatively small percentage of error.

5.2 Problem statement 2 (Square plate with a central circular hole)

The second model for two-dimensional plane stress problem is illustrated in Figure 5(a). In this model, a square plate section was being placed under uniform tensile stress (plane stress) of 100 N/m², acting in a perpendicular direction to the width at the edges of the plate and having a circular hole of diameter 0.1 m at the middle of it. The square plate had a length of 0.5 m, a width of 0.5 m, and a thickness of 0.01 m. The modulus of elasticity and Poisson's ratio of the material of the plate were 210×10^9 N/m² and 0.3 respectively.

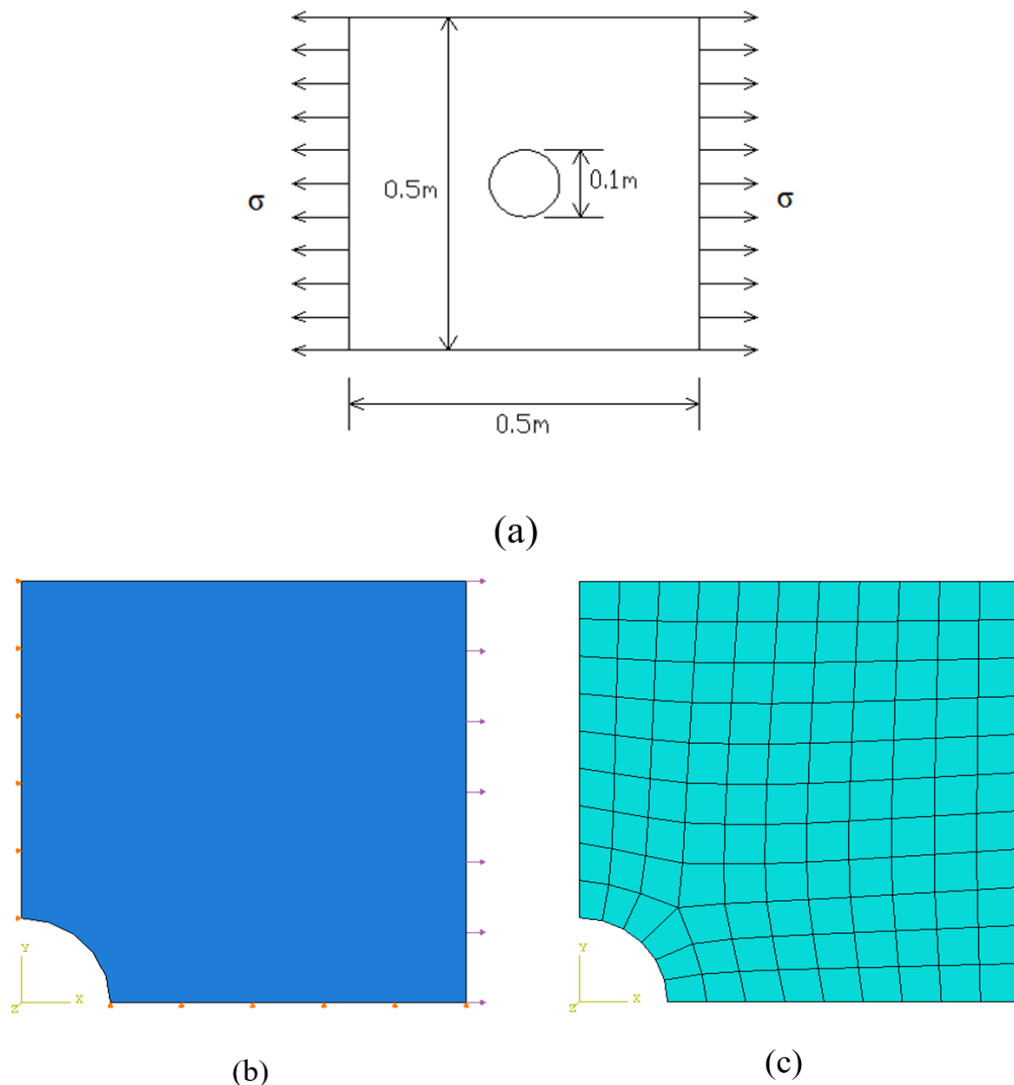


Figure 5: a) Square plate with a central circular hole subjected to uniform tensile stress; b) Application of boundary conditions and loadings; c) Quadrilateral mesh

For modeling purposes, one quarter of the plate was being subjected to analysis due to the symmetrical appearance of the structure about horizontal and vertical axis. Application of uniform stress at the edges was being applied with the help of symmetrical boundary conditions. The geometry of the plate model along with its loading was

symmetrical. Now this symmetric property can be fully utilized by modeling only a quarter portion in which the sides of the quarter of plates adjacent to the hole were being constrained to move in such direction which would restrict the rigid body displacement of the model. The boundary conditions and loadings were applied using the FEA software as shown in Figure 5(b). In this Figure 5(b), the left vertical edge adjacent to the hole was constrained along x direction, i.e., $U_x = 0$ and the bottom horizontal edge adjacent to the hole was constrained along y direction, i.e., $U_y = 0$ and a uniform tensile stress equivalent to 100 N/m^2 was applied to the right vertical edge. The model had 142 nodes and 118 quadrilateral elements. The generated quadrilateral mesh for the model is illustrated in Figure 5(c).

The FEM analysis (results) of second model in terms of σ_{mises} (von-Mises stress) was illustrated in Figure 6(a). From Figure 6(a), it was noted that the σ_{mises} were maximum around the region of element no 1, particularly near the nodes of 2 and 12 which was shown in Figure 6(b). As a computer program was developed for plane stress analysis, the output file for model 2 was obtained using the program in terms of stresses at the four integration points. From Figure 6(b), it was obvious that the σ_{mises} were maximum for element no 1 which consists of node no 1, 2, 12, and 15. Comparison of σ_{mises} , σ_x , σ_y , and τ_{xy} for element no 1 at the four integration points obtained from the developed program and the analysis were shown in Table 3 to Table 6. The most vulnerable region in terms of stresses was found to be around element no1 that consists of node no 1, 2, 12, and 15. So stresses at the four integration points for element no 1 were compared for the second model.

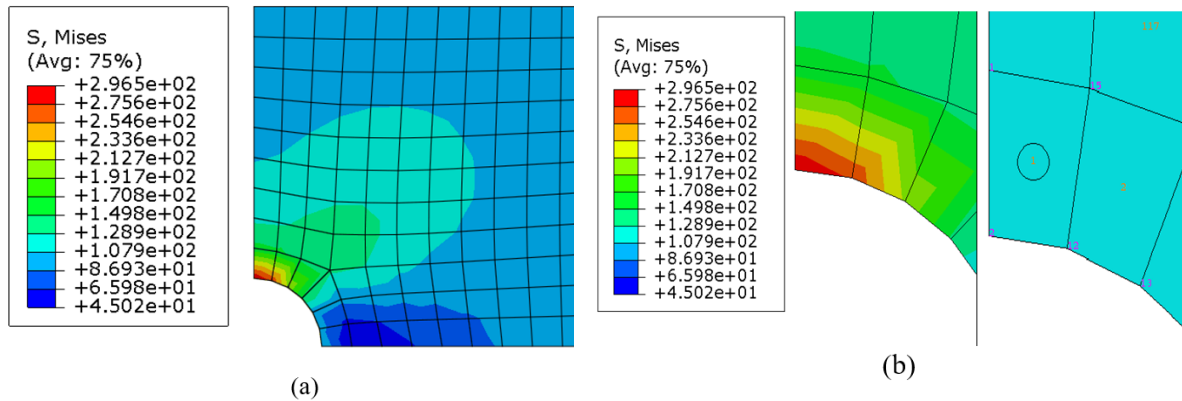


Figure 6: a) Analysis of a square plate with a central circular hole in terms of σ_{mises} ; b) Location of the most vulnerable region in terms of σ_{mises} (element no. 1)

Table 3: Comparison of σ_{mises} for a square plate with a central circular hole

Element No.	Integration point	σ_{mises} from developed program (N/m ²)	σ_{mises} from analysis (N/m ²)	% of error
1	1	1752.590	1810.500	3.304
	2	2546.310	2630.510	3.307
	3	2503.800	2586.590	3.307
	4	1706.440	1762.820	3.304

Table 4: Comparison of σ_x for a square plate with a central circular hole

Element No.	Integration point	σ_x from developed program (N/m ²)	σ_x from analysis (N/m ²)	% of error
1	1	1808.340	1868.090	3.304
	2	2719.420	2809.350	3.307
	3	2646.320	2733.830	3.307
	4	1739.640	1797.110	3.304

Table 5: Comparison of σ_y for a square plate with a central circular hole

Element No.	Integration point	σ_y from developed program (N/m ²)	σ_y from analysis (N/m ²)	% of error
1	1	117.449	121.324	3.299
	2	393.242	406.252	3.308
	3	421.678	435.630	3.309
	4	140.342	144.975	3.301

Table 6: Comparison of τ_{xy} for a square plate with a central circular hole

Element No.	Integration point	τ_{xy} from developed program (N/m ²)	τ_{xy} from analysis (N/m ²)	% of error
1	1	5.386	5.575	3.499
	2	-32.663	-33.734	3.277
	3	-260.822	-269.452	3.309
	4	-191.524	-197.856	3.306

Table 3 presents the values of σ_{mises} , with the maximum tensile stress identified at integration point 2 for element number 1. The developed program yielded a value of 2546.310 N/m², while the analysis provided a value of 2630.510 N/m². These two values were quite similar, with an error of only 3.307%. Upon comparing all the other values in Table 3, it was noted that the σ_{mises} results exhibited a relatively small error of approximately 3.305%. The findings regarding σ_{mises} from previous studies demonstrated a high degree of similarity (Hoque, 2016; Hoque and Islam, 2023).

Upon examination of Table 4, it was observed that the maximum tensile stress, denoted as σ_x , was located at integration point 2 for element number 1. The value obtained from the developed program for σ_x was 2719.420 N/m², while the analysis yielded a value of 2809.350 N/m². These two values were in proximity, with a minimal error of 3.307%. Furthermore, when comparing all the other values in Table 4, it was evident that the results displayed a similar trend, with an error of approximately 3.305%.

Table 5 displays the values of σ_y , with the maximum tensile stress identified at integration point 3 for element number 1. The developed program generated a value of 421.678 N/m², whereas the analysis yielded a value of 435.630 N/m² for σ_y . These two values were relatively close, with an error of approximately 3.309%. While comparing the remaining values in Table 5, it was observed that the results consistently showed a close resemblance, with an error of approximately 3.304%.

In case of τ_{xy} , it was obvious from Table 6 that the maximum compressive stress occurred at the integration point 3 for element no 1 which had a value of 260.822 N/m² obtained from the developed program and 269.452 N/m² obtained from the analysis. These two values were reasonably close, having an error of 3.309%. The tensile stress occurred at the integration point 1 for element no 1 in which the values were 5.386 N/m² utilizing the developed program and 5.575 N/m² obtained from the analysis. These two values were reasonably close, having an error of 3.499%. In comparison with all other values from Table 6, it was noticed that the results were reasonably close, showing an error of about 3.300%.

To visualize the generated mesh for different structural components of a ship, a two-dimensional mesh viewer program has been developed utilizing the Python programming language. Figure 7 showcase the resultant quadrilateral meshes for the above-mentioned model, which includes both the rectangular plate and the square plate with a central circular hole. These meshes have been generated based on the magnification factor computed through the Python program.

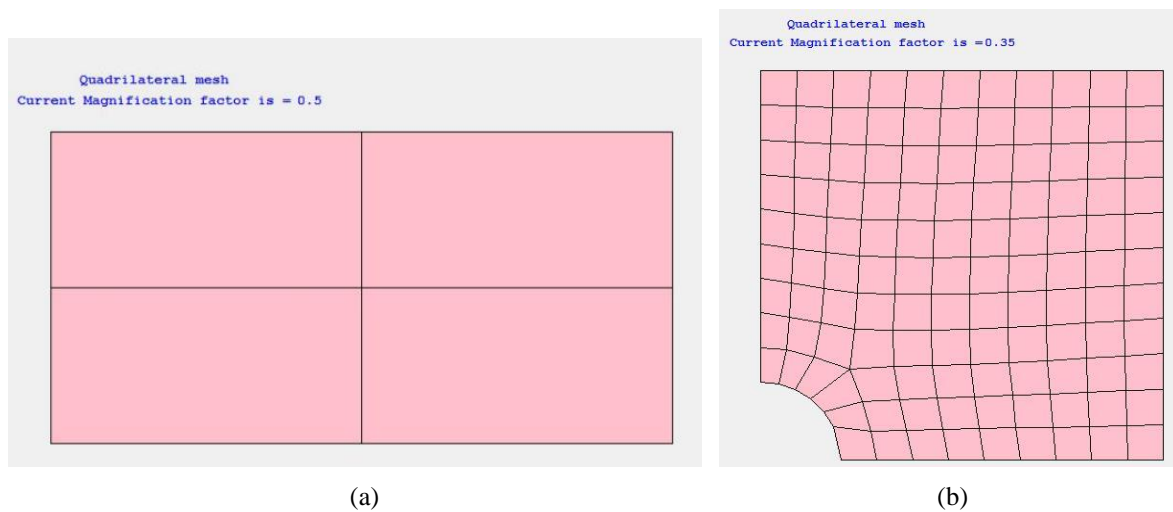


Figure 7: Quadrilateral mesh obtained by using the developed mesh viewer program for a) rectangular plate; b) square plate with a central circular hole.

6. Conclusions

The conclusions that can be made from this study are summarized below:

- An efficient and dependable object-oriented program has been created for two-dimensional, four-node quadrilateral elements. This program enables the accurate determination of stress values at the four integration points (gauss points) for different ship sections containing structural discontinuities. It proves to be a valuable tool for analyzing a wide range of two-dimensional plane stress and plane strain problems, significantly enhancing the analysis process.
- The program developed to analyze the ship sections' most vulnerable region successfully validated the analysis findings. When comparing the stress values at each gauss point, it was observed that the analysis results obtained from the program exhibited only a minimal percentage of error. This demonstrates the high level of accuracy and reliability achieved by the developed program.
- The developed mesh viewer program has the capability to visualize both quadrilateral and triangular meshes, adjusting the magnification factor to accommodate various models associated with ship structural sections.
- This work utilizes FEA software to enhance the understanding of structural discontinuity issues specific to ship structures. By employing FEA software, a deeper comprehension of these problems is achieved, enabling more effective analysis and solutions for ship structural discontinuities.

Acknowledgements

The authors would like to express their sincere gratitude to all the individuals who have provided their valuable support, both directly and indirectly, throughout various phases of this project. Furthermore, the authors would like to highlight the UGC HEQEP Sub Project "Strengthening the Research Capabilities and Experimental Facilities in the Field of Marine Structure" (CP#3131), which has significantly contributed to the enhancement of the simulation lab facilities.

References

- Baugh, J.W., and Rehak, D.R. (1990): Computational abstractions for finite element programming, Technical Report R-89-182, Department of Civil Engineering, Carnegie Mellon University, Pittsburgh, USA.
- Baumann, G.W. (1997): Linear structural stress analysis of a hull girder penetration and a short longitudinal bulkhead using finite element modeling. M.Sc. Thesis, Naval Postgraduate School, Monterey, California, USA.
- Bea, R.G., Cramer, E., Schulte-Strauthaus, R., Mayoss, R., Gallion, K., Ma, K., Holzman, R., and Demsetz, L. (1995): Ship's Maintenance Project. Conducted at University of California, Berkeley for US Coast Guard, Ship Structure Committee (SSC), SSC-386.

- Desjardins, R., and Fafard, M. (1992): Developpement d'un logiciel pour l'analyse des structures par elements finis utilisant l'approche de la programmation orientee objets. Rapport GCT-92-05, Universite Laval, Sainte-Foy, Canada.
- Dubois-Pelerin, Y., Zimmermann, T., and Bomme, P. (1992): Object-oriented finite element programming, A prototype program in Smalltalk. *Comput. Methods Appl. Mech. Engrg.* 98, pp. 361-397.
- Edholm, A. (2013): Meshing and visualization routines in the python version of CALFEM. Master's Dissertation, Lund University, Sweden.
- Fenves, G.L. (1990): Object-oriented programming for engineering software development. *Engrg. with Comput.* 6, pp. 1-15.
- Forde, B.W.R., Foschi, R.O., and Stiemer, S.F. (1990): Object-oriented finite element analysis. *Comput. & Structures* 34, pp. 355-374.
- Hoque, K. N., and Presuel-Moreno, F. (2023): Accelerated Corrosion of Steel Rebar in Concrete by Electromigration: Effect of Reservoir Length and Concrete Mixes. *Proceedings of the 13th International Conference on Marine Technology (MARTEC 2022)*. <https://doi.org/10.2139/ssrn.4446360>.
- Hoque, K. N., and Presuel-Moreno, F. (2023): Corrosion Propagation of Steel Rebar Embedded in Marine Structures Prepared with Binary Blended Concrete Containing Slag. *Proceedings of the 13th International Conference on Marine Technology (MARTEC 2022)*. <https://doi.org/10.2139/ssrn.4447455>.
- Hoque, K. N., and Presuel-Moreno, F. (2023): Corrosion Behavior of Reinforcing Steel Embedded in Fly Ash Concrete. *Proceedings of the 13th International Conference on Marine Technology (MARTEC 2022)*. <https://doi.org/10.2139/ssrn.4447479>.
- Hoque, K. N., and Presuel-Moreno, F. (2023): Corrosion of Steel Rebar Embedded in Ternary Blended Concrete Exposed to High Humidity Environment. *Proceedings of the 13th International Conference on Marine Technology (MARTEC 2022)*. <https://doi.org/10.2139/ssrn.4447482>.
- Hoque, K. N., and Islam, M. S. (2023): Stress-strain analysis of structural discontinuities associated with ship hulls. *Journal of Naval Architecture and Marine Engineering (JNAME)*, Vol. 20(1), pp. 37-51.
- Hoque, K. (2020): Corrosion propagation of reinforcing steel embedded in binary and ternary concrete. Ph.D. Dissertation, Department of Ocean and Mechanical Engineering, Florida Atlantic University (FAU), Boca Raton, Florida, USA.
- Hoque, K. (2016): Analysis of structural discontinuities in ship hull using finite element method. M.Sc. Thesis, Department of Naval Architecture and Marine Engineering, Bangladesh University of Engineering and Technology (BUET), Dhaka, Bangladesh.
- Mackerle, J. (2000): Object-oriented techniques in FEM and BEM. a bibliography (1996-1999), *Finite Elements in Analysis and Design*, Vol. 36, pp. 189-196.
- Martha, L.F. (2002): An object-oriented framework for finite element programming. in *Fifth World Congress on Computational Mechanics*, Austria.
- Miller, G.R. (1991): An object-oriented approach to structural analysis and design. *Comput. & Structures* 40, pp. 75-82.
- Niu, M.C. (1998): *Airframe Structural Design*. Conmilit Press Ltd., Hong Kong.
- Presuel-Moreno, F., Hoque, K., and Rosa-Pagan, A. (2022): Corrosion propagation monitoring using galvanostatic pulse on reinforced concrete legacy samples, 2020-FAU-02 Final Report for National University Transportation Center TriDurLE.
- Presuel-Moreno, F., and Hoque, K. (2019): Corrosion propagation of carbon steel rebar embedded in concrete. *NACE Corrosion 2019 Conference & Expo*, Nashville, Tennessee, USA.
- Presuel-Moreno, F., Nazim, M., Tang, F., Hoque, K., and Bencosme, R. (2018): Corrosion propagation of carbon steel rebars in high performance concrete. BDV27-977-08 Final Report for Florida Department of Transportation (FDOT) Research Center.
- Rahman, M.M., Biswas, M.A.S., and Hoque, K.N. (2022): Recent development on micro-texturing of UHMWPE surfaces for orthopedic bearings: A review, *Biotribology*, vol. 31, pp. 1-10.
- Soares, C.G., and Garbatov, Y. (1998): Reliability of maintained ship hull girders subjected to corrosion and fatigue. *Struct. Saf.* 20, pp. 119-201.
- Thohura, S., and Islam, M.S. (2013): Study of the effect of finite element mesh quality on stress concentration factor of plates with holes, *International Journal of Engineering and Innovative Technology (IJEIT)*, vol. 3, Issue 6, pp. 82-88.
- Zimmermann, T., Dubois-Pelerin, Y., and Bomme, P. (1992): Object-oriented finite element programming, Governing principles. *Comput. Methods Appl. Mech. Engrg.*, vol. 98, pp. 291-303.